Computation of Three-Dimensional Boundary Layers on Fuselages

E.H. Hirschel*
Messerschmitt-Bölkow-Blohm GmbH, Ottobrunn, Federal Republic of Germany

A new approach is developed to construct boundary-layer coordinates, and to handle metric properties, transformations, and so forth on realistic configurations. The approach, which employs tensorial concepts, is discussed in its major steps. Results of boundary-layer computations on a helicopter body, a car body, and on a supersonic fighter nose found with the integral method of COUSTEIX are then used to show the potential of the approach. Special attention is given to the interpretation of the boundary-layer results with regard to possible separation patterns. The results may be used in order to model separated flow.

Introduction

METHODS for the computation of laminar or turbulent three-dimensional boundary layers have been available for several years. Comparisons of integral and finite-difference methods, as well as applications to test cases organized for instance by the EUROVISC-Working Party on Three-Dimensional Shear Layers,[1,2] have established an acceptable level of confidence for applications in design aerodynamics.

Boundary-layer computations on simple wing geometries are made routinely today. The computation of boundary layers on general configurations, especially fuselage configurations, has been hampered because of the problems connected with the creation of boundary-layer coordinates on the surfaces of such configurations. Recently, means have been developed for the definition of general, nonorthogonal, curvilinear boundary-layer coordinates,[3,4] so that boundary-layer theory can now be applied in design aerodynamics to flows on rather complicated shapes.

In the present paper a brief description is given of some of the concepts obtained in Ref. 3 with regard to boundary-layer problems on fuselages. Results of boundary-layer studies on a helicopter fuselage, a car body, and on a supersonic fighter nose are discussed in order to show the value of the approach.

Because three-dimensional boundary-layer separation is difficult to detect in computations, some ad hoc criteria are applied: $|\tau|-$ minimum criterion,[5] convergence of skin-friction lines, and bulging of boundary-layer thickness and displacement-thickness contours.[6] Special attention is given to the interpretation of the boundary-layer results with regard to possible separation patterns, which may be used in order to model separated flow. The above separation criteria, together with topological laws and details of the skin-friction distribution, allow one in many cases to sketch the skin-friction line topology beyond the region where boundary-layer results were found; that is, the separation region.

The boundary-layer method used for the studies is the integral method of COUSTEIX[7] in the form of COUSTEIX-AUPOIX. In this method a mixing length model is used together with similarity solutions to find families of both main-flow and cross-flow profiles. The continuity equation is applied as an entrainment equation. The surface is assumed to be insulated. The method is formulated for arbitrary boundary-layer coordinates and can be applied to flows with Mach numbers up to $M=4$. The resulting set of integral relations is solved by means of a method of lines, which employs a Runge-Kutta scheme in the x^1 direction.

The inviscid flowfields for the first two applications (helicopter, car) were computed with the MBB Panel method,[8] and for the supersonic case with an Euler code.[9] The geometry representation, the construction of the boundary-layer coordinates, the computation of the metric tensor, and the transformation of the external inviscid flowfield was made with the MBB-3D-BL-Geometry method,[10] which is based on the concepts in Ref. 3. The evaluation of the results of the boundary-layer method (displacement thickness, equivalent inviscid source distribution, skin-friction lines, etc.) was made with the MBB-3D-BL-Evaluation method,[11] which is also based on the concepts in Ref. 3.

Basic Concepts of Geometry Handling

For sufficiently slender fuselages, cross-section boundary-layer coordinates can be employed conveniently.[3,4] (It is, however, possible to use coordinates not oriented at the fuselage cross sections.) Consider a fuselage, Fig. 1, which is embedded in a Cartesian reference-coordinate system ($x^{i'}$ system, $i'=1,2,3$). Boundary-layer (surface) coordinates (x^α system, $\alpha=1,2$) are arranged in such a way that cross sections comprise lines of constant x^1, where the Gaussian parameter x^1 is measured along the Cartesian $x^{1'}$ axis with $x^1=0$ at the nose and $x^1=1$ at the rear of the fuselage. The upper symmetry line of the fuselage serves as the datum line for the circumferential (cross-section) direction with the other Gaussian parameter $x^2=0$ in the upper symmetry line, $x^2=0.5$ in the lower, and $x^2=1$ again in the upper symmetry line.

The basic relations which connect the boundary-layer coordinate system and the Cartesian reference-coordinate system are[3,4]

$$x^{1'}=L_{x^1}x^1 \tag{1a}$$

$$x^{2'}=x_o^{2'}(x^1)+L_{x^2}(x^1)\int_0^{x^2}\cos\alpha_c(x^1,\xi^2)\,d\xi^2 \tag{1b}$$

$$x^{3'}=x_o^{3'}(x^1)-L_{x^2}(x^1)\int_0^{x^2}\sin\alpha_c(x^1,\xi^2)\,d\xi^2 \tag{1c}$$

where L_{x^1} ($L=$ body length in most cases) is the normalizing length for the $x^2=$constant coordinate, $L_{x^2}(x^1)$ (circumferential length of the cross section) the normalizing length for the $x^1=$constant coordinate, $x_o^{2'}(x^1)$ and $x_o^{3'}(x^1)$ the coordinates of the datum line (usually $x_o^{2'}\equiv 0$ on fuselages), and $\alpha_c(x^1,x^2)$ the contour angle (see Fig. 1).

Submitted Nov. 4, 1982; revision received March 23, 1983.

*Aeronautics Engineer. Member AIAA.

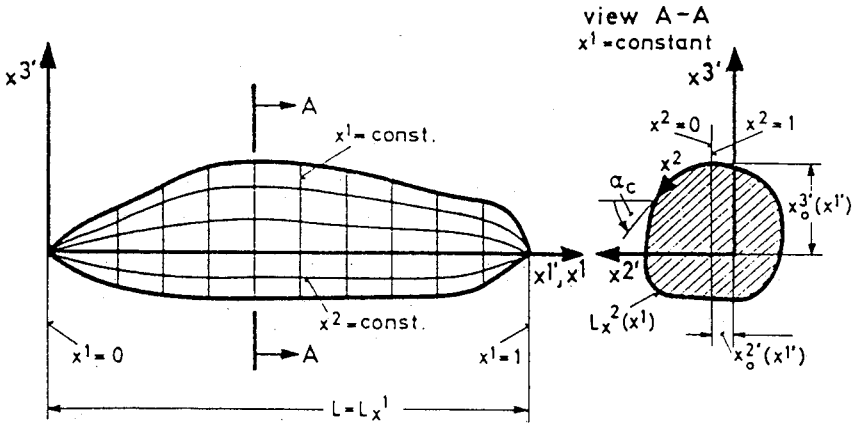

Fig. 1 Schematic of cross-section coordinates.[4]

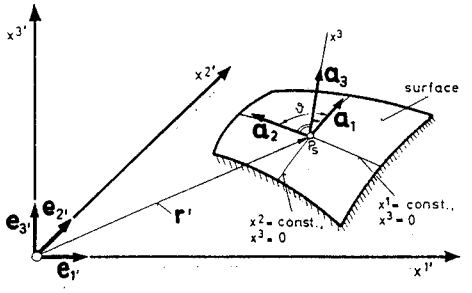

Fig. 2 Surface element with base vectors.

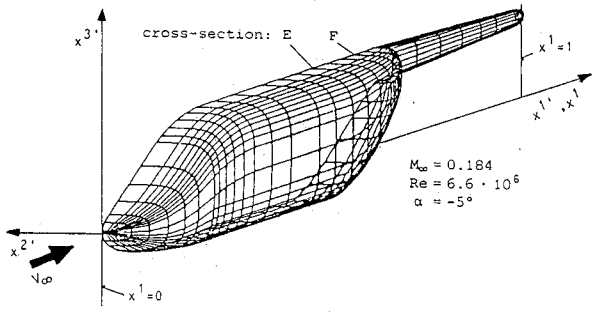

Fig. 3 Schematic of helicopter fuselage (left half).

With these relations, the components $\beta_\alpha^{i'}$ of the base vectors a_α ($\alpha=1,2$), Fig. 2, of the x^α system can be computed[3,4]:

$$\beta_\alpha^{i'} = \frac{\partial x^{i'}}{\partial x^\alpha} \tag{2}$$

The components $\beta_3^{i'}$ of the third base vector a_3 are found from the conditions $a_3 \cdot a_\alpha = 0$, $|a_3| = 1$ (boundary-layer coordinates are a special case of locally monoclinic surface-oriented coordinates[3]).

The components of the metric surface tensor $(a_{\alpha\beta})$ are then computed with

$$a_{11} = (\beta_1^{1'})^2 + (\beta_1^{2'})^2 + (\beta_1^{3'})^2 \tag{3a}$$

$$a_{12} = a_{21} = \beta_1^{1'}\beta_2^{1'} + \beta_1^{2'}\beta_2^{2'} + \beta_1^{3'}\beta_2^{3'} \tag{3b}$$

$$a_{22} = (\beta_2^{1'})^2 + (\beta_2^{2'})^2 + (\beta_2^{3'})^2 \tag{3c}$$

In literature often the Lamé coefficients h_1, h_2, g are used; the relation is:

$$(a_{\alpha\beta}) = \begin{bmatrix} (h_1)^2 & g \\ g & (h_2)^2 \end{bmatrix} \equiv \begin{bmatrix} a_{11} & a_{12} \\ a_{21} & a_{22} \end{bmatrix} \tag{4}$$

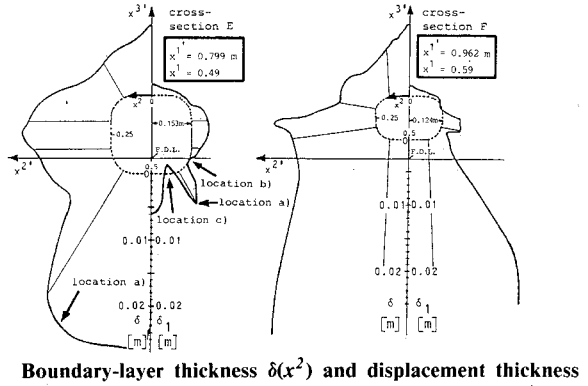

Fig. 4 Boundary-layer thickness $\delta(x^2)$ and displacement thickness $\delta_1(x^2)$ at cross sections *E* and *F*.

The angle ϑ between the coordinate lines, Fig. 2, is related to the metric coefficients by

$$\cos\vartheta = \frac{a_{12}}{\sqrt{a_{11}}\,\sqrt{a_{22}}} \tag{5}$$

The velocity components of the external inviscid flowfield, which are usually computed in the Cartesian reference coordinate system can be transformed into the x^α system with the relations[3]

$$v_e^\alpha = \beta_i^\alpha v_e^{i'} = \beta_1^\alpha v_e^{1'} + \beta_2^\alpha v_e^{2'} + \beta_3^\alpha v_e^{3'} \tag{6a}$$

$$v_e^3 = \beta_i^3 v_e^{i'} \overset{!}{=} 0 \tag{6b}$$

where the Jacobian β_i^j ($j=\alpha,3$) is the inverse of the matrix $\beta_j^{i'}$. The velocity components v_e^α are contravariant components. They are related to the physical components $v_e^{*\alpha}$ by

$$v_e^\alpha = \frac{v_e^{*\alpha}}{\sqrt{a_{(\alpha\alpha)}}} \tag{7}$$

External inviscid streamlines and skin-friction lines on the body surface are defined in the same way as in Cartesian coordinates[3]:

$$\frac{dx^1}{v_e^1} = \frac{dx^2}{v_e^2} \tag{8a}$$

$$\frac{dx^1}{\tau_w^1} = \frac{dx^2}{\tau_w^2} \tag{8b}$$

where $\tau_w^\alpha = \tau_w^{*\alpha}/\sqrt{a_{(\alpha\alpha)}}$ are the contravariant components of the skin-friction vector.

Friction forces finally are found from[3,6]

$$\Delta R^\alpha = \tau_w^\alpha dF = \tau_w^\alpha \sqrt{a}\, dx^1 dx^2 \tag{9}$$

with a the determinant of the metric tensor, Eq. (4). The transformation into the $x^{i'}$ system is made with [summation convention as in Eq. (6)]:

$$\Delta R^{i'} = \beta^{i'}_{\alpha} \Delta R^{\alpha} \tag{10}$$

Boundary-Layer Results

The methods mentioned in the Introduction, some of which[10,11] employ the concepts sketched in the preceding section, were applied to several fuselage configurations. In the following, boundary-layer results are given for a helicopter fuselage, a car body, and a supersonic fighter nose. Details of the computations, like the metric properties, outer boundary data, skin-friction distributions, etc., are given in internal company reports,[12-14] respectively. In all cases, approximate initial conditions were used, which, if placed in regions with sufficiently favorable pressure gradients, soon lose their influence on the solution. In this way problems with the singularity of the metric at $x^1 = 0$, which always exists, and the problems which occur if the stagnation point does not lie at $x^1 = 0^3$, are avoided.

Helicopter Fuselage

Figure 3 shows the left side of a helicopter configuration which was investigated in a wind tunnel. The boundary-layer study was made for the wind tunnel situation with the flow parameters given in Fig. 3. Because the fuselage was considered at an angle of attack $\alpha = -5$ deg, the upper symmetry line is a weak attachment line. The boundary-layer thickness δ and the displacement thickness δ_1 therefore have a relative maximum at the upper symmetry line, Fig. 4. This also leads to an accumulation of boundary-layer material at the lower side of the fuselage. The bulge of δ at $x^2 \approx 0.4$ (location a), as well as the peak of δ_1, indicates a convergence of skin-friction lines which can be seen in Fig. 5. This is accompanied by a divergence of skin-friction lines at $x^2 \approx 0.35$ and $x^2 \approx 0.44$ (locations b and c) in cross-section E. (At cross-section F the flow already has separated and no data are given for the lower side.) All this and the existence of a $|\tau|$-minimum line[5] (not shown in Fig. 5) indicate the presence of a vortex-layer separation line.[6]

This vortex-layer separation line is also present in the experiment, although it lies somewhat upstream of the computed separation line, Fig. 6. This is due to the fact that neither the local nor the global interaction of separated and inviscid flow was taken into account in the computation at the aft end of the fuselage.

In Fig. 6 the oil-flow picture (a) compares well with the computed skin-friction lines (b). In the experiment laminar-turbulent transition takes place partly in a small separation bubble at the nose. The laminar calculation failed there, but the turbulent calculation, which was started at $x^1 = 0.03$, shows no separation at that point, and is in very good agreement up to the aft end of the fuselage where the general separation occurs.

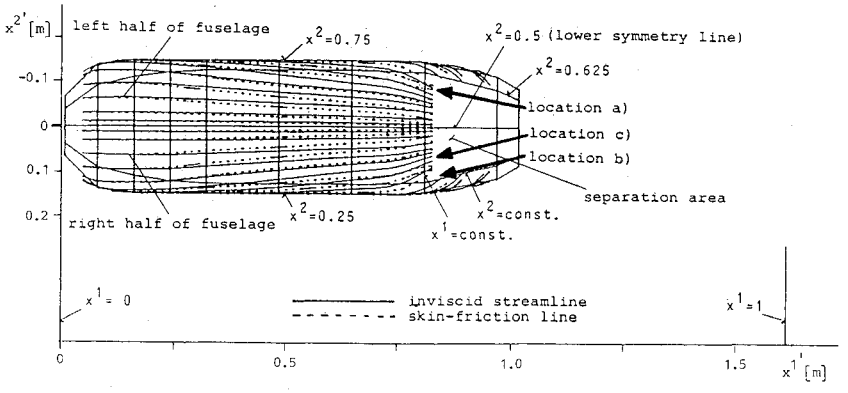

Fig. 5 Inviscid streamlines and skin-friction lines at the helicopter surface seen from below.

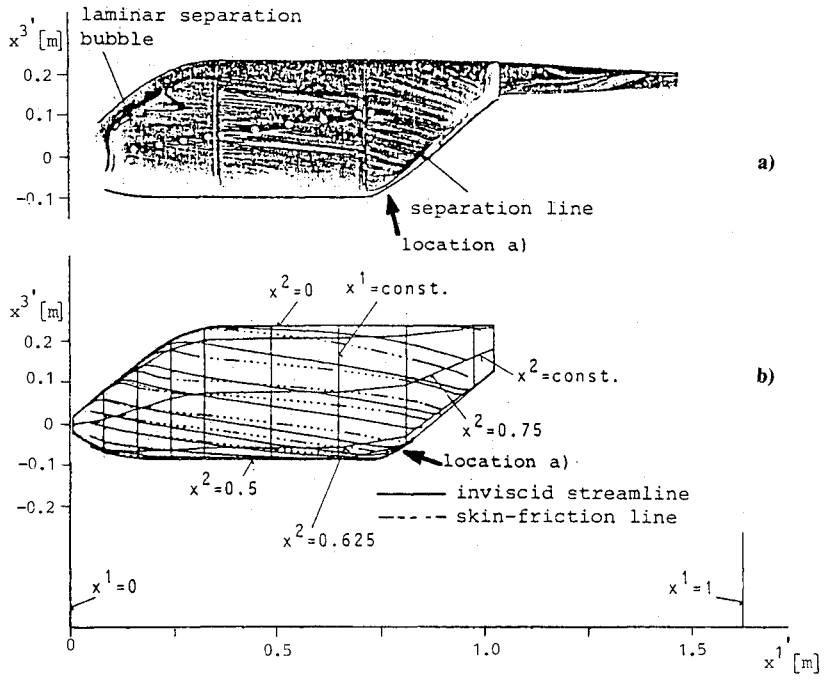

Fig. 6 Side view of helicopter fuselage (left half): a) oil-flow picture; b) inviscid streamlines and skin-friction lines.

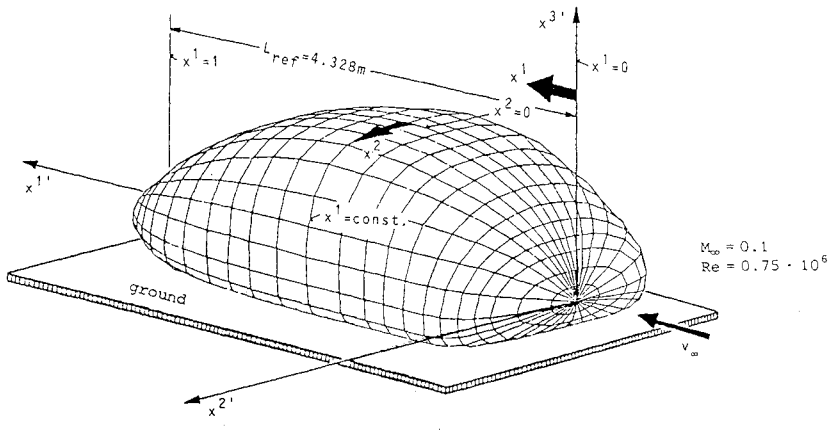

Fig. 7 Schematic of car body (SCHLOER car).

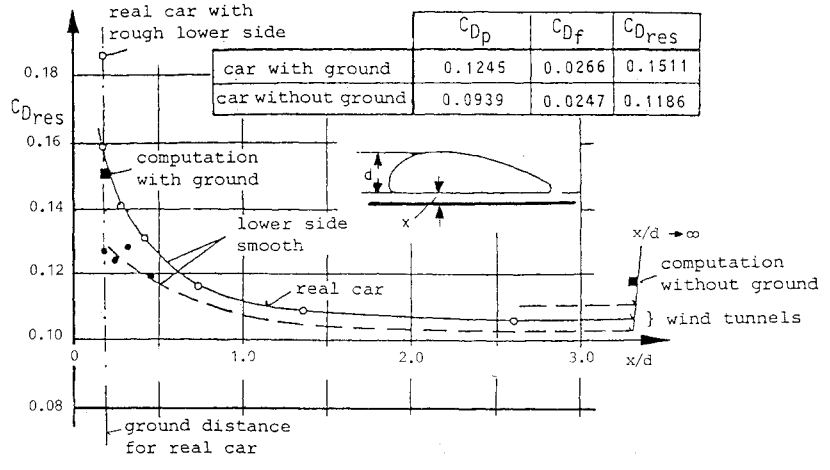

Fig. 8 Comparison of computed data (■), and experimental data (wind tunnels: --, ●; real car test -, ○).

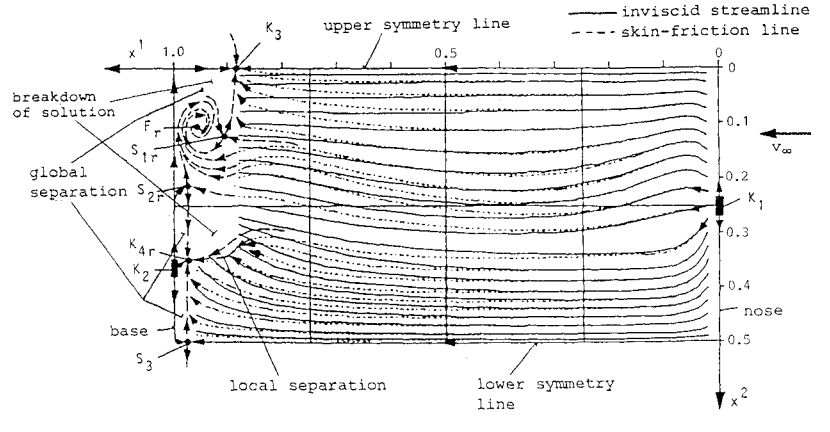

Fig. 9 Possible topology of separated flow in the x^α-plane (K = nodal point, S = saddle point, F = focal point), right half of body with ground.

Car Body

In the late 1930s at the AVA Göttingen, the flow past an automobile which had an exceptionally good aerodynamic shape, Fig. 7, was studied by K. Schloer. For this car the boundary layer was computed with the flow data given in Fig. 7. Two cases were considered: the car in the presence of the ground, and the car without the presence of the ground. The boundary-layer computation broke down in both cases around $x^1 \approx 0.9$. The pressure field was integrated over the whole body assuming $p = p_\infty$ in the area where no boundary-layer solution was found (for the car with ground see Fig. 7). This area was considered to be the base separation area. The resulting pressure drag c_{D_p} for the two cases is shown in the insert in Fig. 8, as well as the friction drag c_{D_f}. The resulting drag $C_{d_{res}}$ compares well with the experimental data in both cases.

This good agreement was, of course, found only because the separation area is small and only rather weak vortices and vortex sheets leave the base, resulting in small pressure changes, interactions, induced drag, etc. Cars today have rather large cutoff areas, which give rise to much stronger effects.[15] In order to gain more insight into the separated flow region, an attempt was made to interpret the results with regard to the skin-friction line topology.[16,17]

The computed skin-friction line pattern for the right half of the car in the presence of the ground is given in the x^α plane in Fig. 9. Convergence of skin-friction lines in the lower rear part, together with a bulging of the boundary-layer thickness contours (not shown here), points to a vortex-layer separation line—local separation[16]—on each side of the car. The convergence of the skin-friction lines at $x^1 \approx 0.9$ in the upper symmetry line, together with $\tau_w \to 0$ at this station,[13] indicates

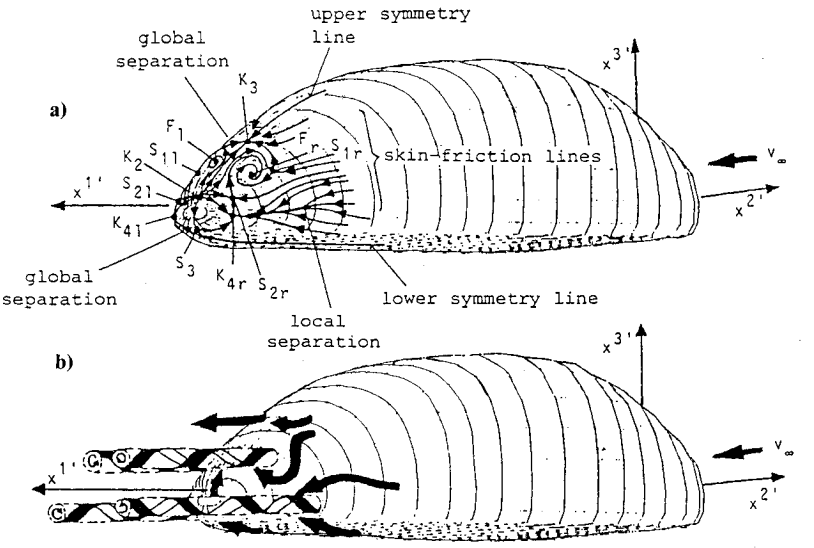

Fig. 10 Separation on real surface: a) possible separation topology; b) possible vortex pattern.

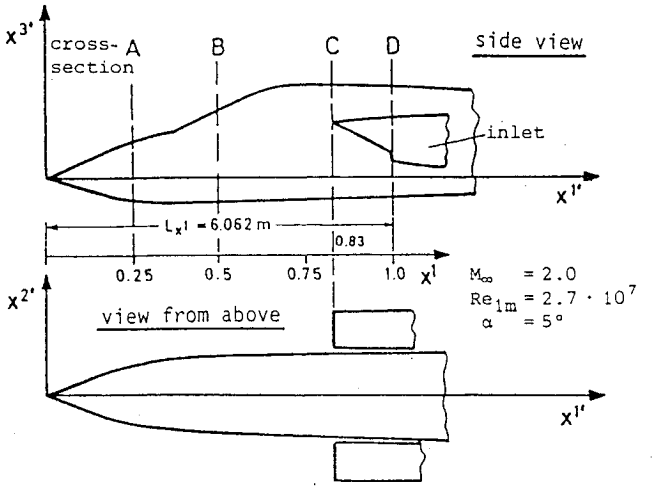

Fig. 11 Schematic of fighter nose.

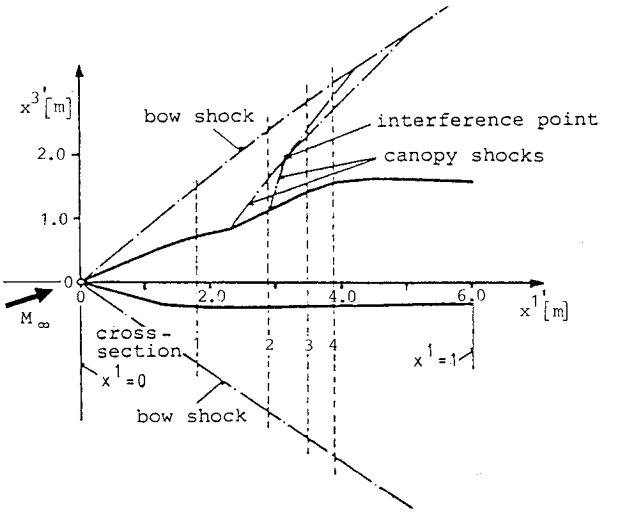

Fig. 12 Location of bow shock and embedded shocks at $M_\infty = 2$.

the existence of the singular point K_3 in Fig. 9, which is a nodal point. The other skin-friction line pattern points to the existence of a focal point F on each side at the back of the car, which is also seen in experiments. The separation pattern shown in Fig. 9 was deduced using the topological law for skin-friction lines[16] that on the surface of a body the number of nodal (here $N=5$) and focal (here $F=2$) points exceeds the number of saddle points (here $S=5$) by two.

In (Fig. 10a) the flow pattern is given at the surface of the car; Fig. 10b shows the possible vortex configuration. It appears that two pairs of vortices leave the base (Fig. 10b), although the near wake undoubtedly is much more complicated. Older visualization tests have shown only the lower pair to exist, the upper probably being very weak.

Supersonic Fighter Nose

The boundary-layer development on a fighter nose, Fig. 11, up to the inlet was studied for a flight Mach number $M_\infty = 2$, and a Reynolds number per meter $Re_{1m} = 2.7 \cdot 10^7$. The inviscid flowfield computation[9,18] yields not only the outer boundary values for the boundary-layer computation, but also the location of the bow shock and the locations of embedded shocks (Figs. 12 and 13). For the boundary-layer computation only the total-pressure loss due to the bow shock, which is attached to the conical nose for the given Mach number, was taken into account. Embedded shocks can be corner shocks, like the canopy shock, or recompression shocks, like the cross-flow shocks seen at cross section 4 in Fig. 13. The first usually begin at the surface and interact with the boundary layer; the latter often form at a certain distance from the surface and, therefore, do not directly affect the boundary layer, at least they do not reduce the total pressure at the surface.

In Fig. 14 the distribution of the total skin-friction coefficient c_f is given. It exhibits a prominent dip at the front of the canopy, but shows, in general, that the shock waves computed in Ref. 18 obviously are smeared out sufficiently (or are far enough away from the surface) so that no local separation regions are found.

In reality, the picture may be different, but in principle, by using more mesh points, the Euler code[9] is able to capture the shock waves much more sharply, so that the boundary-layer computation can detect possible local separation areas.

In Fig. 15 the inviscid streamlines and the skin-friction lines show the general development of the flow. The direction of the external flow was verified by experimental data at three stations at cross section C. In Fig. 16 the boundary-layer thickness and the displacement thickness are given. The data show reasonable agreement with experimental data (1:20 model) scaled to the present free-flight computation conditions. The position of the boundary-layer diverter appears to be slightly too close to the fuselage.

In Fig. 17 the cumulated friction forces are finally shown. The force R' in the x' (axis) direction rises monotonously,

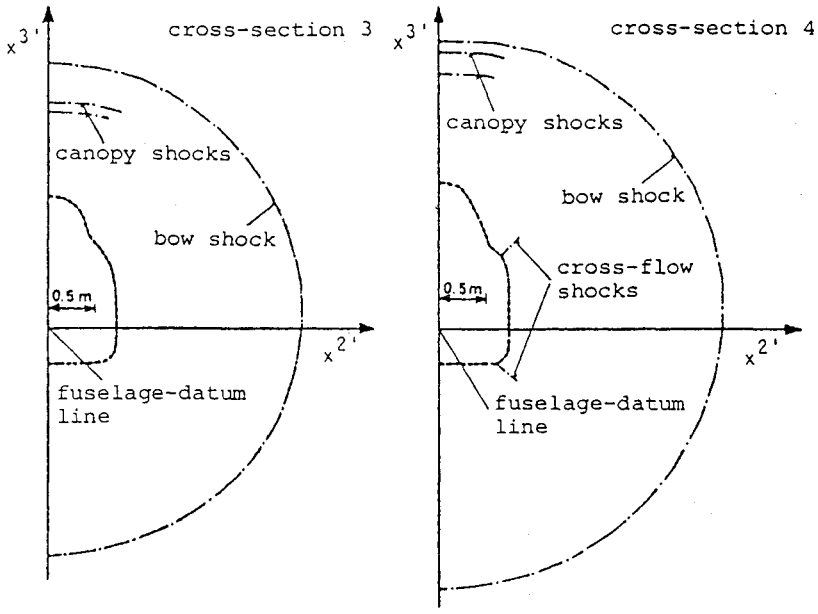

Fig. 13 Location of shocks in cross sections 3 and 4 (see Fig. 12) at $M_\infty = 2$.

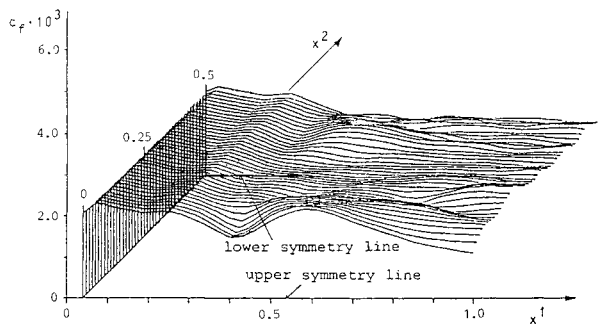

Fig. 14 Distribution of skin-friction coefficient $c_f(x^\alpha)$ (right half of fuselage).

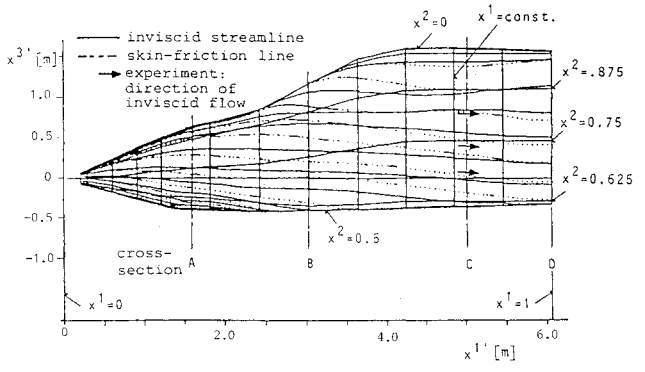

Fig. 15 Side view of fighter nose: inviscid streamlines, skin-friction lines, inviscid flow direction from experiment (left half of fuselage).

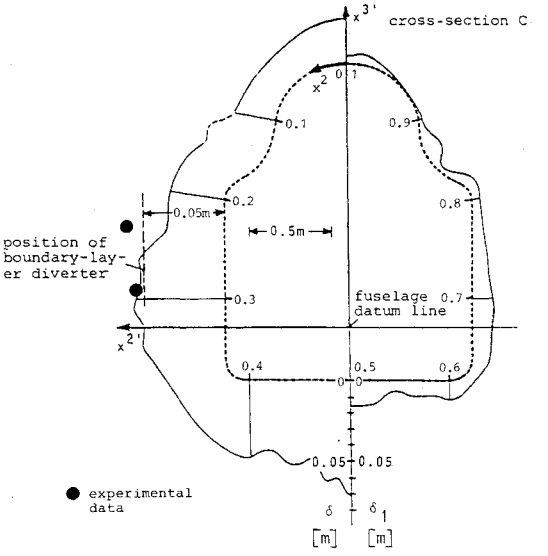

Fig. 16 Boundary-layer thickness $\delta(x^2)$ and displacement thickness $\delta_1(x^2)$ at cross section C (see Fig. 11).

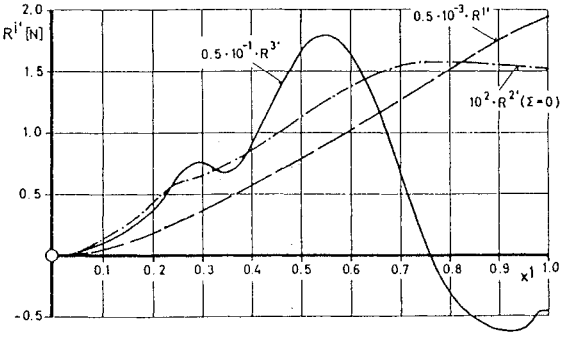

Fig. 17 Cumulated friction forces $R^{i'}(x^1)$; $R^{1'}$ and $R^{3'}$ for complete configuration, $R^{2'}$ for right half of configuration.

whereas the force $R^{3'}$ is first directed upward and then downward. The small friction force $R^{2'}$ in the $x^{2'}$ direction is, of course, compensated, due to the symmetry of the configuration, by the force on the other half.

Conclusions

A new approach to handle the geometrical problems connected with theoretical boundary-layer investigations on realistic configurations is outlined. Results of boundary-layer computations on fuselage configurations show that very detailed investigations can be made, and that important clues can be found with regard to the separation behavior of the boundary layer. This is true even if local or global interactions between separating boundary layer and inviscid flowfield are not taken into account.

The boundary-layer computations were made with the integral method of COUSTEIX. In the few cases in which

experimental data are available for comparison, the agreement is satisfactory. However, in order to establish a higher degree of realibility, additional and more detailed experimental data are necessary.

With boundary-layer theory, of course, the flow in such complicated separation regions as those appearing on bluff rear bodies cannot be computed. Boundary-layer theory can give important clues in some cases about the location of vortex-layer separation lines, which may be used in Euler simulations of the separated flowfield. Recently, such methods have been developed (see, for instance Refs. 19 and 20) for flows past wings with sharp edges (swept leading edge, trailing edge), where the separation location is fixed. Separation location means, in this context, the location where the vorticity carrying boundary-layer flow leaves the surface. The vorticity shed in this way is then arranged, in some cases, into very complicated assemblages of vortices.

In principle, the Euler equations can describe the transport and arrangement of vorticity. However, it remains to be seen how important secondary and higher separation phenomena (which topological studies and experiments show to exist), and diffusion effects are inside separation regions. Nevertheless, it is hoped that together with boundary-layer solutions, Euler simulations can be used to compute the pressure drag of a configuration, at least in those cases where the pressure drag makes up the major part of the total drag.

References

[1] Humphreys, D.A., "Comparison of Boundary-Layer Calculations for a Wing," The May 1978 Stockholm Workshop Test Case, EFA TN AE-1522, Jan. 1979; also, *AIAA Journal* Vol. 19, No. 2, 1981, pp. 232-234.

[2] Lindhout, J.P.F., van den Berg, B., and Elsenaar, A., "Comparison of Boundary-Layer Calculations for the Root Section of a Wing," The September 1979 Amsterdam Workshop Test Case, NLR MP 80028 U, 1981.

[3] Hirschel, E.H. and Kordulla, W., *Shear Flow in Surface-Oriented Coordinates,* Vieweg Verlag, Braunschweig 1981, Vol. 4 of *Notes on Numerical Fluid Mechanics.*

[4] Hirschel, E.H., "Boundary-Layer Coordinates on General Wings and Fuselages," *ZFW,* Zeitschrift tuad Flugwissenschatten und Weltraumforschung Vol. 6, Heft 3, 1982, pp. 194-202.

[5] Hirschel, E.H. and Kordulla, W., "Local Properties of Separation Lines," *ZFW,* Vol. 4, 1980, pp. 295-307.

[6] Hirschel, E.H., "Three-Dimensional Boundary-Layer Calculations in Design Aerodynamics," *Proceedings of IUTAM-Symposium on Three-Dimensional Turbulent Boundary Layers,* Fernholz, H.H. and Krause, E. eds., Springer Verlag, Berlin-Heidelberg-New York, 1982, pp. 353-365.

[7] Cousteix, J., "Integral Method and Turbulence Models Applied to Three-Dimensional Boundary Layers," *Proceedings of IUTAM-Symposium on Three-Dimensional Turbulent Boundary Layers,* Fernholz, H.H. and Krause, E. eds., Springer Verlag, Berlin-Heidelberg-New York, 1982, pp. 286-297.

[8] Kraus, W. and Sacher, P., "The Panel Method for the Computation of the Pressure Distribution on Configurations at Subsonic Speed," *ZFW,* Vol. 21, 1973, pp. 303-311.

[9] Weiland, C., "Calculation of Three-Dimensional Stationary Supersonic Flow Fields by Applying the 'Progonka' Process to a Conservative Formulation of the Governing Equations," *Journal of Computational Physics,* Vol. 29, No. 2, Nov. 1978, pp. 173-198.

[10] Hirschel, E.H., "A Method for the Processing of Initial, Boundary, and Metric Data for the Computation of Three-Dimensional Boundary Layers with the Methods of COUSTEIX" MBB/FE122/S/R/1530, 1982.

[11] Hirschel, E.H., "A Method for the Computation of Wall Shear-Stress Components, Three-Dimensional Displacement Thickness, Equivalent Inviscid Source Strength, and Skin-Friction Lines from the Results of the Methods of Cousteix," MBB/FE122/S/R/1546, 1982.

[12] Hirschel, E.H., "Boundary-Layer Computation for a Helicopter Fuselage," MBB-UFE122-AERO-MT-547, 1981.

[13] Hirschel, E.H. and Bretthauer, N., "Boundary-Layer Computations for the Schloer Automobile," MBB-UFE122-AERO-MT-577, 1982.

[14] Hirschel, E.H., "Boundary-Layer Computation for the Foward Part of the Tornado Fuselage," MBB-UFE122-AERO-MT-578, 1982.

[15] Hirschel, E.H., Bretthauer, N., and Röhe, H., "Theoretical and Experimental Boundary-Layer Studies on Car Bodies," *Proceedings of Symposium on Vehicle Aerodynamics,* Wolfsburg, Federal Republic of Germany, Dec. 1982.

[16] Peake, D.J. and Tobak, M., "Three-Dimensional Interactions and Vortical Flows with Emphasis on High Speeds," NASA TM 81 169, 1980; also AGARDograph 252, 1980.

[17] Dallmann, U., "Topological Structures of Three-Dimensional Flow Separation," DFVLR IB 221-82 A 07, 1982.

[18] Weiland, C., "The Computation of Inviscid Supersonic Flow Fields Past Arbitrary Airplane Fuselages," MBB-UFE122-AERO-MT-548, 1981.

[19] Eriksson, L.E. and Rizzi, A., "Computation of Vortex Flow around Wings using the Euler Equations," *Proceedings of fourth GAMM Conference on Numerical Methods in Fluid Dynamics,* edited by H. Viviand, Vieweg, Braunwschweig 1981, Vol. 5 of *Notes on Numerical Fluid Mechanics,* pp. 87-105.

[20] Weiland, C., "Vortex Flow Simulation past Wings using the Euler Equations," AGARD CP 342, 19-1 to 19-12, 1983.